ARTICLE OPEN ACCESS

Application of Electrical Resistance Probes for Corrosion Monitoring and Cathodic Protection Assessment of Offshore Structures

Mohammad Hassanzadeh[1,2] | Nicolas Larché[1] | Erwan Diler[1] | Johan Becker[1] | Barbara Rossi[2,3] | Raf Dewil[2,3]

[1]French Corrosion Institute, Brest, France | [2]KU Leuven, Department of Chemical Engineering, Leuven, Belgium | [3]University of Oxford, Department of Engineering Science, Oxford, UK

Correspondence: Nicolas Larché (nicolas.larche@institut-corrosion.fr)

Received: 8 January 2026 | **Revised:** 13 February 2026 | **Accepted:** 12 March 2026

Funding: Horizon Europe Marie Skłodowska-Curie Actions, Grant/Award Number: 101073471

Keywords: corrosion monitoring | ER probe | offshore structures | seawater | sensor

ABSTRACT

An innovative electrical resistance probe was developed for in-situ, real-time corrosion monitoring of offshore structures, featuring a 1.0 mm track thickness and five sensing tracks. The increased thickness improves compatibility with industrial materials, while the additional tracks provide a more qualitative assessment of non-uniform corrosion. The probe's performance was evaluated under submerged exposure in natural seawater and across anodic to cathodic potentials, simulating galvanic couplings and varying levels of cathodic protection. Its monitoring results were benchmarked against conventional weight-loss coupons, and the effect of corrosion product accumulation on probe functionality was examined. The probe delivered accurate corrosion rates and confirmed its reliability in natural seawater. The increased thickness extended service life and provided a corrosion-depth sensitivity of 70 nm, while the greater number of tracks brought the exposed area closer to that of coupons, improving detection of non-uniform corrosion. The probe also detected, in real time, variations in corrosion rate caused by interruptions in the cathodic protection system.

1 | Introduction

1.1 | Background

Monitoring the initiation and progression of corrosion is essential for effective maintenance planning and timely intervention, potentially reducing associated damage costs by 15%–35% [1, 2]. This need is especially critical for remote offshore structures exposed to harsh marine conditions [3, 4]. In offshore structures, the exposure zones are commonly categorized into four levels: atmospheric, splash, submerged, and buried. According to DNV-RP-0416, corrosion protection strategies for these structures generally involve a combination of cathodic protection (CP), protective coatings, and corrosion allowance [5].

Therefore, any corrosion monitoring technique employed must demonstrate consistent and reliable performance across these diverse environmental conditions. Given that the cathodic protection system serves as the final ring of defense in the corrosion protection hierarchy, complementing both coatings and material selection, continuous monitoring of CP performance is essential to ensure the structural integrity.

Corrosion monitoring differs from inspection in both frequency and methodology. While inspections are conducted periodically at predetermined intervals, monitoring involves continuous or near-continuous evaluation of corrosion activity [6, 7]. For unmanned remote offshore assets, such as wind turbines and seaweed farms, corrosion monitoring techniques should possess the following characteristics: (i) durability in harsh seawater

environments, (ii) capability for online (continuous) monitoring, (iii) capability for real-time monitoring, (iv) provision of quantitative corrosion measurements, at least for general corrosion, and (v) applicability under both immersed and atmospheric conditions. Under such circumstances, preference is given to methods that are cost-effective and user-friendly in terms of both operation and data interpretation [7–9].

As shown in Figure 1, corrosion monitoring techniques are generally classified into direct and indirect methods. Indirect techniques do not provide quantitative measurements of corrosion rates [10–13]. Quantitative assessment of corrosion requires direct monitoring techniques, which are typically divided into two categories: electrochemical and physical methods [11, 14].

All corrosion monitoring techniques have their specific drawbacks. In terms of electrochemical techniques, these drawbacks are the difficulty of using them in atmospheric condition [2, 6, 8, 9, 11, 15–17] or in systems with high corrosion rates or low electrolyte conductivity [1, 13, 18], electrode bridging [13, 18], interfering currents or potential generated by electrochemically active species [6, 13, 14], being sensitive to diffusion-controlled conditions [1, 2, 8, 19], difficulty of localized corrosion interpretation [1, 4, 6, 8, 11, 13, 14, 18], weakness in corrosion rate quantification [13, 19], and restricted field practicality [1]. Even CMAS as a modern electrochemical technique has its specific restrictions [20].

Direct physical techniques are characterized by similar drawbacks. Some of them, such as CC, OSP, IPT, UT, GW, RT, IRT, THz, MW, and various electromagnetic techniques do not provide real-time or online monitoring [2, 10, 21, 22]. Others like QCM, FOCS and RFID are not practical for harsh offshore environments [13, 15, 22, 23] or like AE [11, 21, 24], FSM [25–27] and RPERS [24, 28, 29] are limited to specific applications due to their inherent features and complexities.

ER probes can provide quantitative corrosion rates by monitoring changes in electrical resistance caused by the reduction of the cross-sectional area due to corrosion. This monitoring technique allows ER probes to operate effectively in both wet and dry conditions. In addition to their technical advantages, ER probes are generally more cost-effective than other corrosion monitoring sensors available on the market [7, 20].

Although ER probes have certain limitations, their low cost, ease of operation and data interpretation, compatibility with a wide range of environments, and ability to provide quantitative and real-time data make them a suitable choice for corrosion monitoring of offshore structures and for assessing the performance of their cathodic protection (CP) systems which are the subject of this study. This selection is consistent with previous findings reported in the literature [9, 30–35].

1.2 | ER Probe Principles

Since their development in the 1950s [36, 37], ER probes have been manufactured in a variety of geometries, including wire, tube, strip, loop, and thin-sheet forms, and are available in different thicknesses and materials [16]. The electrical resistance (ER) technique operates by detecting an increase in the electrical resistance of a metal element as it corrodes, which directly corresponds to the loss of its cross-sectional area. The underlying principle of this technique is based on Ohm's law, where the electrical resistance R (in ohms, Ω) of a metal element is expressed by Equation (1) [38]:

$$R = \frac{\rho L}{A} = \frac{\rho L}{wt}, \tag{1}$$

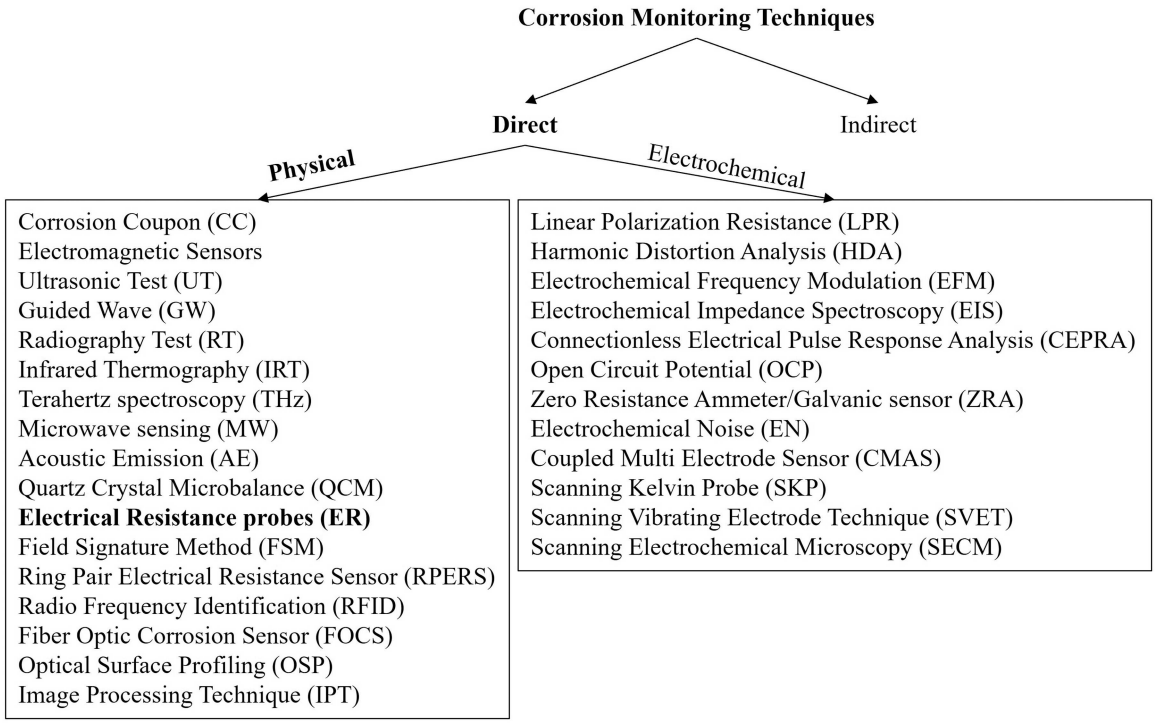

FIGURE 1 | Classification of corrosion monitoring methods into indirect and direct approaches.

where ρ is the specific electrical resistivity of the metal (temperature-dependent), expressed in Ω·m; L is the length of the current path (in meters); w is the width (in meters); and t is the thickness (in meters), as illustrated in Figure 2. Monitoring is carried out by applying a very small current through the ER probe, small enough to avoid affecting the probe temperature [2, 23], while measuring the potential difference along the probe to determine its electrical resistance. By tracking changes in the electrical resistance over time, the loss in metal thickness due to corrosion and consequently, the corrosion depth (CD) can be quantified. The corrosion rate, defined as the rate of change in corrosion depth over time, can thus be continuously monitored [7, 38].

The ER probes are usually designed with two distinct elements: a sensing part that is exposed to the corrosive environment, and a reference part that is isolated from corrosion exposure. Since the electrical resistance of metals is also affected by temperature, the resistance ratio between the measuring element exposed to corrosion and the resistance of a similar reference element protected from corrosion is measured to compensate for resistivity changes due to temperature which is reflected in Equations (2) and (4) [6, 13, 38].

Conventional ER probes such as those ones used by Legat et al. (280 μm thickness) [39], Rosborg et al. [40] (35 μm thickness and 0.5 mm width), Prosek et al. [41, 42] (50 nm–250 μm thickness and 1–2 mm width), Kosec et al. [43] (250 μm thickness and 0.7 mm width), and Thierry et al. [44, 45] (250 μm thickness) are designed with metal tracks that are significantly thinner in thickness than in width. Due to this geometry, when corrosion occurs uniformly across the surface, material loss along the narrow edges has a negligible effect on the overall electrical resistance. Instead, the resistance change is predominantly governed by the reduction in the track's thickness. Therefore, the influence of edge corrosion is minimal, and the variation in resistance primarily reflects uniform thinning across the wider surface area. Based on this principle, Equation (2) is employed to calculate the general corrosion depth of thin-track ER probes [35]:

$$CD = t_{ref,i}\left[\left(\frac{R_{ref,i}}{R_{sens,i}}\right) - \left(\frac{R_{ref}}{R_{sens}}\right)\right], \tag{2}$$

where, CD is the corrosion depth, $t_{ref,i}$ is the initial thickness of the reference track, $R_{ref,i}$ is the initial resistance of the reference track, $R_{sens,i}$ is the initial resistance of the sensing track, R_{ref} and R_{sens} are the resistances of the reference and sensing tracks, respectively, measured as a function of time.

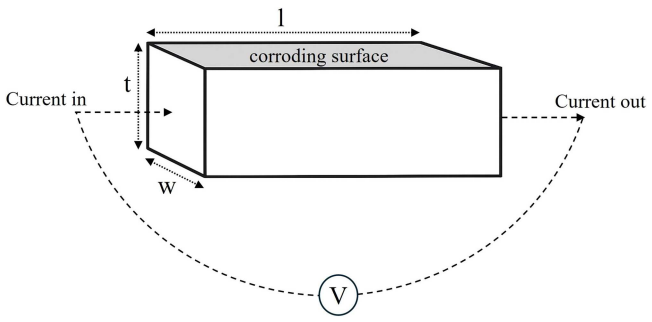

FIGURE 2 | ER measurement principle.

Sensitivity of an ER probe defines how much the measured electrical resistance changes for a given amount of corrosion depth (resistance sensitivity in mΩ/μm), or equivalently, how much thickness change corresponds to a unit change in resistance (*thickness sensitivity* $= \partial CD/\partial R_{sens}$ in μm/mΩ). It expresses the probe's ability to translate resistance variations into corrosion depth. The resolution and sensitivity of an ER probe depend on many factors, such as the quality of instrument, data processing, measurement frequency, environmental conditions and probe design [46, 47].

Using the resolution of resistometer (σ_{Rsens}: the smallest detectable resistance change) and substituting the probe sensitivity ($\partial CD/\partial R_{sens}$) in equation (3), the minimum measurable corrosion depth (σ_{CD}) can be expressed as:

$$\sigma_{CD} = \frac{\partial CD}{\partial R_{sens}}\sigma_{R_{sens}}. \tag{3}$$

The corresponding response time is the duration needed for metal loss to exceed the probe's sensitivity at a given corrosion rate [46]. It is calculated by dividing the minimum measurable corrosion depth by the actual corrosion rate.

The service life of the ER probe is generally defined as the time required for the effective thickness, often taken as half of the original thickness, to be lost due to corrosion. Indeed, when the metallic section becomes very thin and thus resistive, the resistance of the corrosion products layer and/or those of the electrolyte might no longer be negligible [35].

2 | Experimental

2.1 | Materials and Design

All ER probes and coupons were fabricated by cutting 1 mm thick sheets of DC01 cold-rolled mild carbon steel. The nominal chemical composition of DC01, as specified in the EN 10130 standard [48], is provided in Table 1. DC01 was selected as the initial material to assess the effectiveness of the newly developed probe geometry. For broader applicability, future studies should employ probes made from alternative materials, particularly Q355, a key structural steel used in wind turbine components [49].

Figure 3 exhibits the ER probe developed in this study having the isolated reference and the exposed sensing parts. The choice of an appropriate probe geometry considering the environment aggressiveness depends on the desired service life, response time, and measurement sensitivity [38]. Increasing the thickness of the probe extends its service life and response time and reduces its sensitivity [50]. In environments with moderate to high corrosion rates, it is generally advisable to use probes with relatively lower sensitivity and extended service life [1].

In the ER probe developed in this study, track thickness and width are 1.0 mm and 1.8 mm, respectively. The increased

TABLE 1 | The standard chemical composition of DC01 mild carbon steel according to EN 10130.

Max. of elements (%wt)	%C	%Mn	%P	%S
Content	0.120	0.600	0.045	0.045

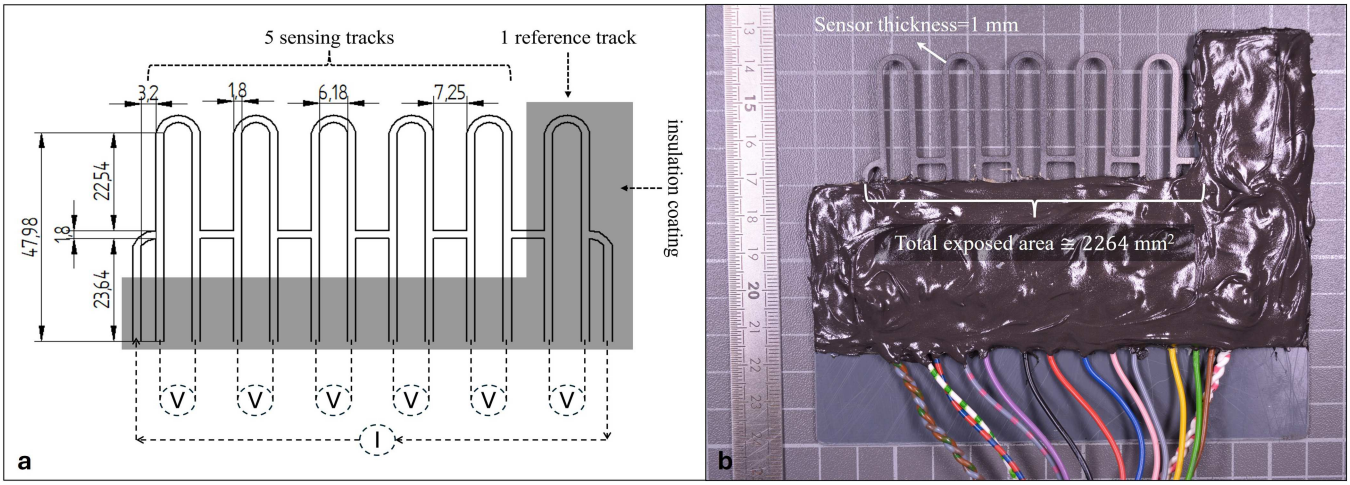

FIGURE 3 | (a) Design of the developed ER probe (all dimensions are in mm), (b) The actual sensor used in this study. [Color figure can be viewed at wileyonlinelibrary.com]

thickness aims to extend the service life of the probe under harsh marine conditions [32, 33] and to enable direct fabrication from industrial materials regardless of thickness. Furthermore, the substrate beneath the probe tracks was removed to minimize the probe size, reduce manufacturing cost, and enhance sensitivity. Therefore, a new corrosion depth calculation approach is required as, (i) the thickness-to-width ratio is no longer negligible and (ii) the absence of a substrate leads to both faces of the probe being exposed. As a result, Equation (4) was established to calculate the corrosion depth (CD) considering the new geometry and edge effect:

$$CD = \frac{1}{4}(t_i + w_i)\sqrt{\frac{R_{ref,i}}{R_{sens,i}}} - \frac{1}{4}\sqrt{\left(t_i^2 + w_i^2\right)\frac{R_{ref,i}}{R_{sens,i}} + 2t_i w_i\left(\frac{2R_{ref}}{R_{sens}} - \frac{R_{ref,i}}{R_{sens,i}}\right)}, \quad (4)$$

where the contributing parameters are defined as in equation (2), and w_i represents the initial track width. Given that non-uniform corrosion occurs sporadically and over small areas, a larger sensor area improves the likelihood of detecting such events thereby enhancing the statistical reliability of the measurements [51]. In addition, enlarging the total exposed surface area of ER probe to approximately ~2264 mm^2, that is, roughly half of one coupon exposed area, ~4709 mm^2, results in a response that is more comparable to that of standard corrosion coupons.

As can be seen in Figure 3, the H-shaped bridge design has been used in this study. In H-shaped bridge design, the edge of the protective coating passes approximately through the center of the bridge. As a result, this edge does not overlap with either the sensing or reference tracks; instead, the bridge functions solely as a current conductor. The sensing segment is positioned at a safe distance from the coating boundary, mitigating a common issue in ER probes, namely, corrosion at the interface beneath the protective coating between the sensing and reference tracks, which can lead to inaccurate readings [2, 41, 52].

All coupons were marked with notches to facilitate post-test identification. Before immersion in seawater, the coupons were cleaned in an ultrasonic bath using heptane for two 10-min cycles, then dried and weighed. After exposure, corrosion products accumulated on both the ER probes and coupons were physically removed and collected for further Raman analysis. Final cleaning was performed according to ISO 8407:2021 standard [53] by running a pickling process in an ultrasonic bath containing 500 mL of 37 wt% hydrochloric acid, 3.5 g hexamethylene tetramine, and the required volume of distilled water to reach 1 L of solution. The process was implemented at 25°C for at least 10 min [6, 54]. The coupons were then reweighed, and the weight loss was used to calculate the corrosion rates.

2.2 | Experimental Setup

In this study, the responsiveness and reliability of the developed ER probe was evaluated under submerged conditions and across a wide range of electrochemical potentials from anodic to cathodic (−650 to − 760 mV vs. Ag/AgCl). This potential range simulates situations in which the cathodic protection system fails to maintain the structure potential above the specified protection acceptance criterion (more anodic potentials), such as gradual consumption of sacrificial anodes in aging structures, insufficient protection in regions remote from the anodes, under-designed protection systems, or interruptions in impressed current cathodic protection systems; as well as the situations where relative protection is obtained (more cathodic). Then, the corrosion rates measured by the ER probes were compared to those determined from weight-loss measurements of coupons exposed under the identical conditions.

As shown in Figure 4, the experimental setup consisted of a single tank continuously filled and drained with natural seawater pumped directly from Brest Bay, France. The flow rate was regulated to achieve a complete water renewal every 24 h. A heater maintained the seawater at a constant temperature of 20 ± 3°C throughout the test period. To ensure homogeneity, the water was continuously circulated within the tank using an internal pump.

The measured variation of other seawater environmental parameters, including salinity, pH, and dissolved oxygen (DO) in Brest Bay is shown by Figure 5. Throughout the test duration, salinity, dissolved oxygen (DO), and pH remained within; narrow ranges of 33–34 (PSU), 8–9 ppm, and 7.75–7.80, respectively.

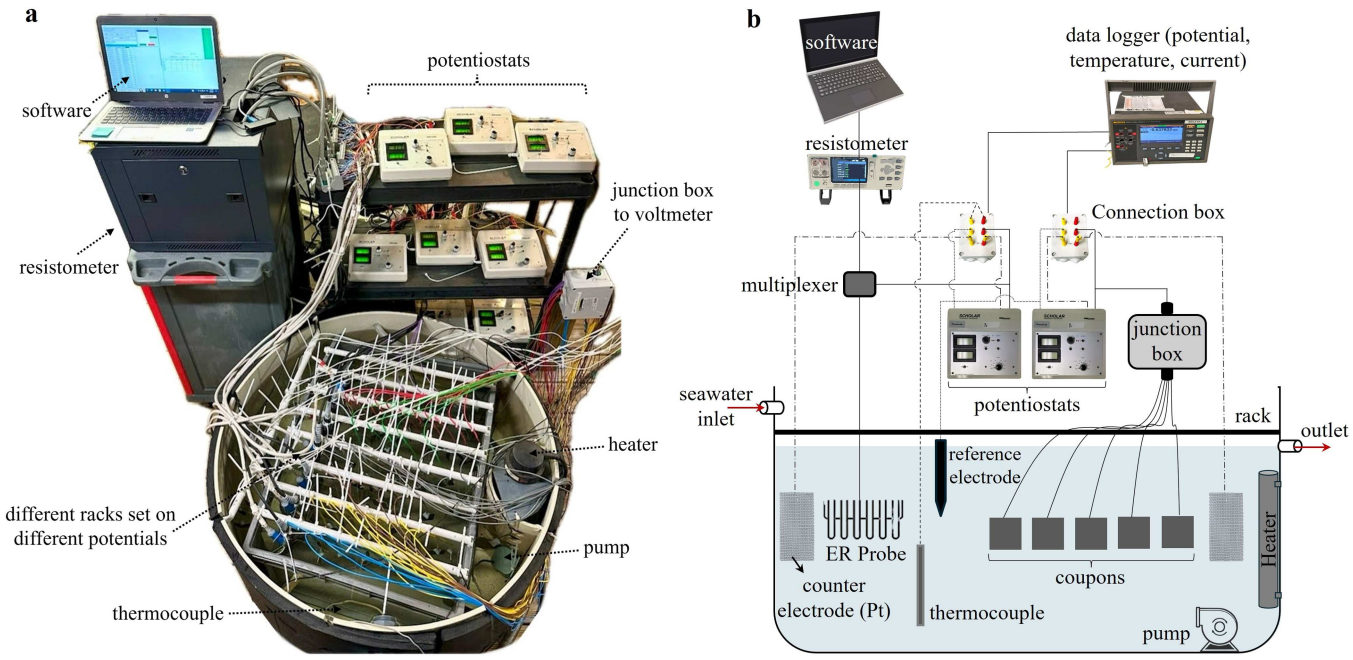

FIGURE 4 | Test setup showing different elements of the experiment. (a) the actual test setup, (b) a schematic exhibiting all connections for one of the racks. [Color figure can be viewed at wileyonlinelibrary.com]

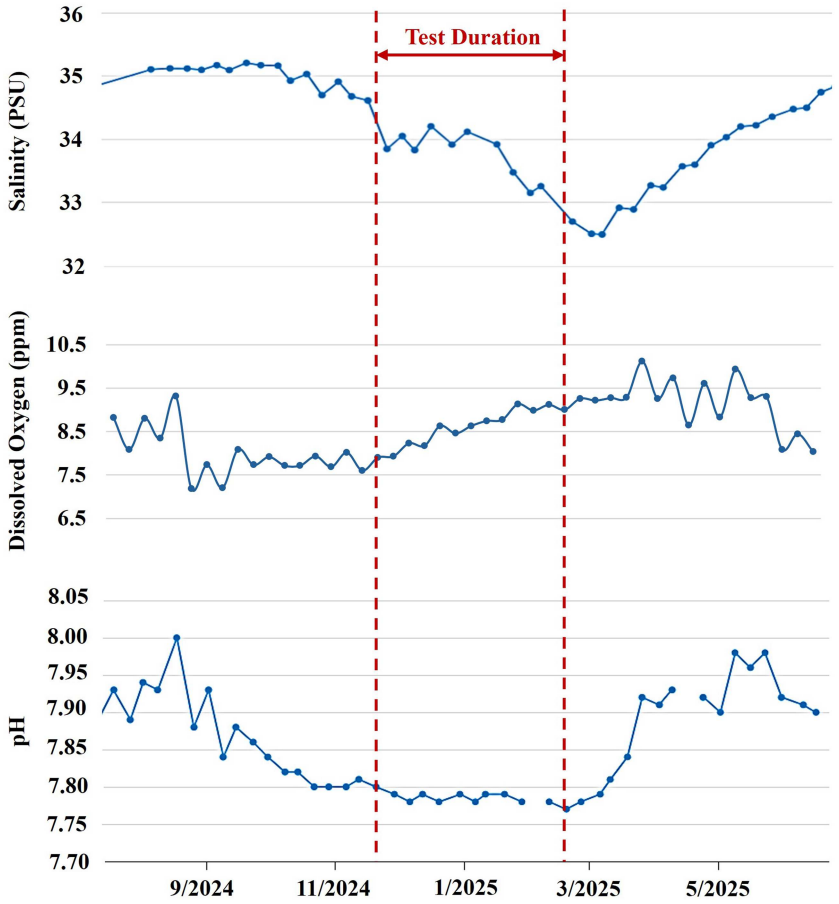

FIGURE 5 | Environmental parameters during the test duration, including salinity, dissolved oxygen, and pH [55]. [Color figure can be viewed at wileyonlinelibrary.com]

As shown by Figure 4, multiple racks were installed inside the tank, each holding one ER probe and five corrosion coupons. The electrochemical potential of the ER probe and associated coupons on each rack was independently controlled using two separate potentiostats. This configuration prevents the formation of a galvanic cell between the probe and the coupons induced by a geometrical factor. Indeed, as experimentally observed in this study, in the same environment the coupons display slightly lower open circuit potential (OCP) and thus act as anode, when interconnected with ER probes which is in line with literature [56].

To eliminate the effects of ohmic drop in the media, a dedicated reference electrode was placed on each rack. All the reference electrodes were Ag-AgCl/KCl-gel electrodes calibrated with a saturated calomel electrode (SCE). A multichannel high impedance voltmeter recorded the actual applied potentials for each ER probe and its corresponding coupon group. A 1-ohm shunt resistor was used on each potentiostat to monitor the applied current required to achieve each set potential.

The ER probes were connected to a resistometer through a multiplexer, which interfaced with a laptop. Electrical resistance measurements were recorded automatically using dedicated software, with a sampling frequency of one reading per hour.

3 | Results and Discussion

For the developed ER probe, by using $t_i = 1000\,\mu m$ and $w_i = 1800\,\mu m$ and calculating $\partial CD/\partial R_{sens}$ at $t = 0$ (initial moment where $R_{ref} = R_{ref.i}$ and $R_{sens} = R_{sens,i}$), the obtained sensitivity is $70\,\mu m \cdot m\Omega^{-1}$. Using equation (3) and a resistometer uncertainty of 4–5 mΩ (±1 μΩ), which represents the resistance range measured under cathodic potentials with the lowest corrosion rates, the corrosion-depth accuracy is ±70 nm. Consequently, in the 5-day intervals for corrosion rate measurements, the corresponding accuracy of corrosion rate is achieved as ±5 μm/year.

Figure 6 presents the electrical resistance versus time curve for the probe under OCP conditions. As shown, the five R_{sens} display a clear upward trend, indicating that their resistance increases due to ongoing corrosion. To pronounce this feature, the effect of temperature was removed from the sensing parts by subtracting the reference ER from the ER of all tacks (ΔR) which is shown by the small graph in Figure 6. Although all five sensing tracks follow a similar overall pattern, their slopes differ. This variation is attributed to the corrosion distribution on the probe surface, where some regions may become more anodic and others more cathodic, resulting in non-uniform corrosion rates. At its maximum, there is a maximum deviation of 16% of the average ER between the two extreme track 5 and 3. Although in the single-track probe the same non-uniform corrosion happens but it is not observable in the measurements due to the single ER reading. Overall, the results indicate that multi-track ER probes may be used to assess both general corrosion rates and trends in maximum non-uniform corrosion. A large difference between the minimum and maximum corroded tracks would be indicative of significant non-uniform attacks. In such cases, general corrosion would be expected to fall between the minimum and mean ER probe values, while the maximum non-uniform corrosion could be estimated from the most corroded ER track. Conversely, when the difference between minimum and maximum track corrosion is small and does not increase significantly over time, this suggests predominantly uniform corrosion with limited non-uniform attack. Under these conditions, the mean corrosion rate from a multi-track ER pobe aligns well with the general corrosion measured on coupons. This finding is in line with the results reported by Refait et al. [57]. The observed trends are promising; nevertheless, future studies incorporating larger sample sets,

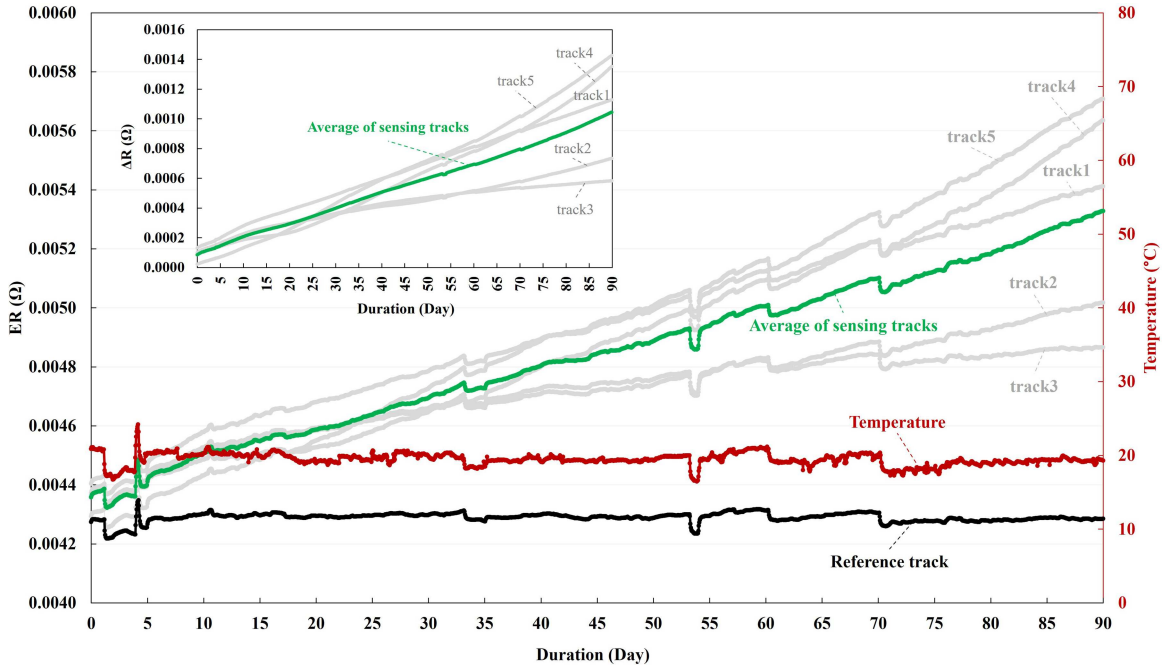

FIGURE 6 | Electrical resistance evolution of the reference and sensing parts of the ER probe under OCP condition in association with the temperature records. The small graph depicts the evolution of Δ R for the sensing tracks achieved by subtracting the reference ER. [Color figure can be viewed at wileyonlinelibrary.com]

extended exposure conditions, and modeling of the multi-track ER probe response under non-uniform corrosion scenarios would help to strengthen and expand these findings.

Figure 7a,b illustrate the corrosion depth evolution of ER probes under OCP and under an anodic polarization condition of −650 mV versus Ag/AgCl, respectively. As shown in Figure 7a, the corrosion depth reached approximately 60 μm after 90 days under OCP condition. In contrast, under the anodic potential of −650 mV versus Ag/AgCl (Figure 7b), the track number 5 of the probe stopped reporting corrosion depth values after 41 days, corresponding to a corrosion depth of nearly 350 μm on each face of the track (700 μm in total). However, the other tracks continued reporting their corresponding corrosion depth values. This shows that the thickness of the fifth track got so thin that its corresponding electrical resistance reached the maximum limit of the measurement range. This confirms again the ability of non-uniform corrosion detection by this ER probe.

For the single-face exposed ER probes, the service life is commonly defined as the time required to reduce the initial track thickness by half [41]. However, as can be seen in Figure 7b for the ER probe of this study under the anodic polarization of −650 mV (vs. Ag/AgCl), the failure in track 5 occurred after a thickness loss of 700 μm and the probe average corrosion depth showed a number close to 600 μm (2 × 300) which is greater than half of the probe thickness (500 μm).

Figure 8 presents the corrosion rate evolution under six different polarization conditions after 90 days. Due to the large disparity in corrosion rates, particularly under −650 mV versus Ag/AgCl and OCP conditions compared to the other applied potentials, the results are displayed using two different vertical scales for clarity. The corrosion rate under the highly anodic condition of −650 mV versus Ag/AgCl reaches approximately 3100 μm/year before failure, whereas it fluctuates around zero with a deviation of 10 μm/year for more cathodic potentials, including −730, −745, and −760 mV versus Ag/AgCl.

The negative corrosion rates registered for the cathodic potentials (blue bullet points in the yellow-shadowed region) are due to very low corrosion rates, i.e. beyond the accuracy of the probe (5 μm/year). Nonetheless, since they are less than 10 μm/year we can consider them in the protection zone (no corrosion), according to ISO 15589-1:2015 [34]. Of course, it should be noted that, since the tank has a limited volume and the racks with different potentials are positioned close to each other, the increased concentration of Fe^{2+} and Fe^{3+} ions generated by the corrosion of coupons and probe at −650 mV versus Ag/AgCl might influence the corrosion rates measured at cathodic potentials [58]. Nevertheless, it should be considered that: first, the concentration of Fe^{2+} and Fe^{3+} in the tank was minimized by continuously filling, draining, and circulating the seawater; and second, the purpose of this study was to assess the performance of the ER probe under cathodic polarization, rather than to obtain precise corrosion rate values under this condition.

Under OCP conditions, the corrosion rate remains relatively stable with a slightly decreasing trend over time. At −715 mV, which is not fully protecting potential, the corrosion rate initially increases and then begins to decline except for a peak between 25 and 30 days. This corrosion rate jump up is attributed to a temporary polarization interruption, as further explained in the following paragraph and Figure 9.

As shown in Figure 9, to evaluate the responsiveness of the ER probe to changes in the CP system, the potentiostat applying the −715 mV potential was deliberately interrupted for 2 days (between days 25 and 27). Deviations in the corrosion rates indicate changes in corrosion conditions [59]. The interruption led to a sharp increase in the average corrosion rate from roughly 20 μm/year (0.0553 μm/day) to 261 μm/year (0.7159 μm/day). Upon reactivation of the potentiostat and restoration of the protective potential, the corrosion rate dropped to 8 μm/year (0.0232 μm/day). These results demonstrate the ER probe's capability to perform online, real-time monitoring of cathodic protection performance. This functionality is particularly valuable for issuing timely alerts in the event of sudden failures in the cathodic protection systems of critical infrastructure or under insufficient polarization.

Figure 10 presents the comparison of corrosion rates measured by the ER probes with those obtained from coupons weight loss for different potential deviations relative to OCP. The table included in Figure 10 additionally summarizes the corrosion rates measured by both the ER probe and the weight-loss coupons at each potential level. Readings at −650 mV were done after 41 days of immersion; OCP values were recorded over

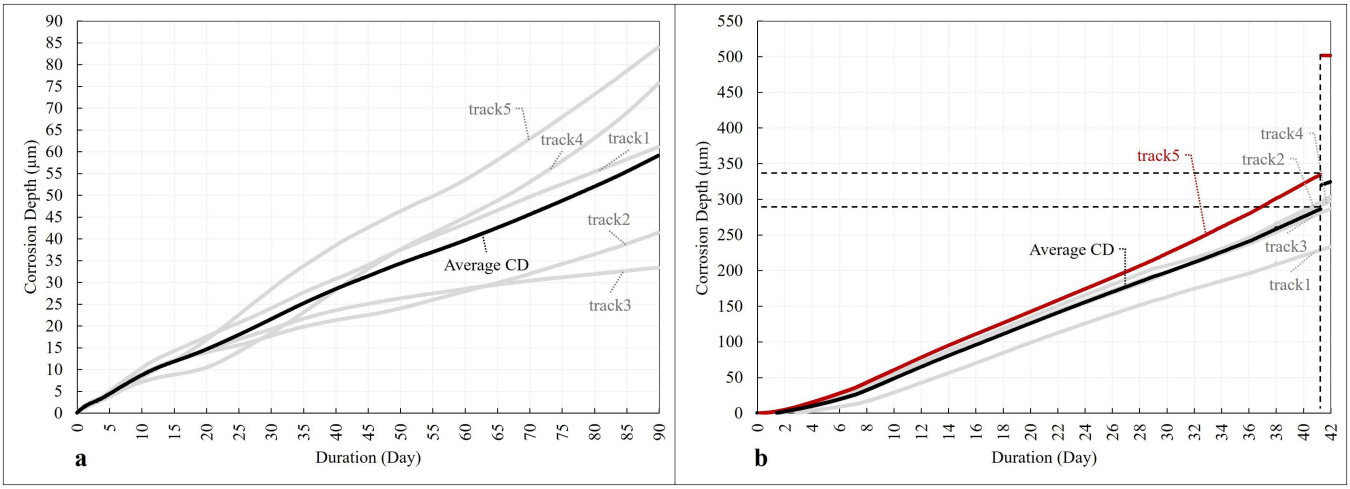

FIGURE 7 | Evolution of corrosion depth under (a) OCP condition and (b) −650 mV versus Ag/AgCl anodic polarization. [Color figure can be viewed at wileyonlinelibrary.com]

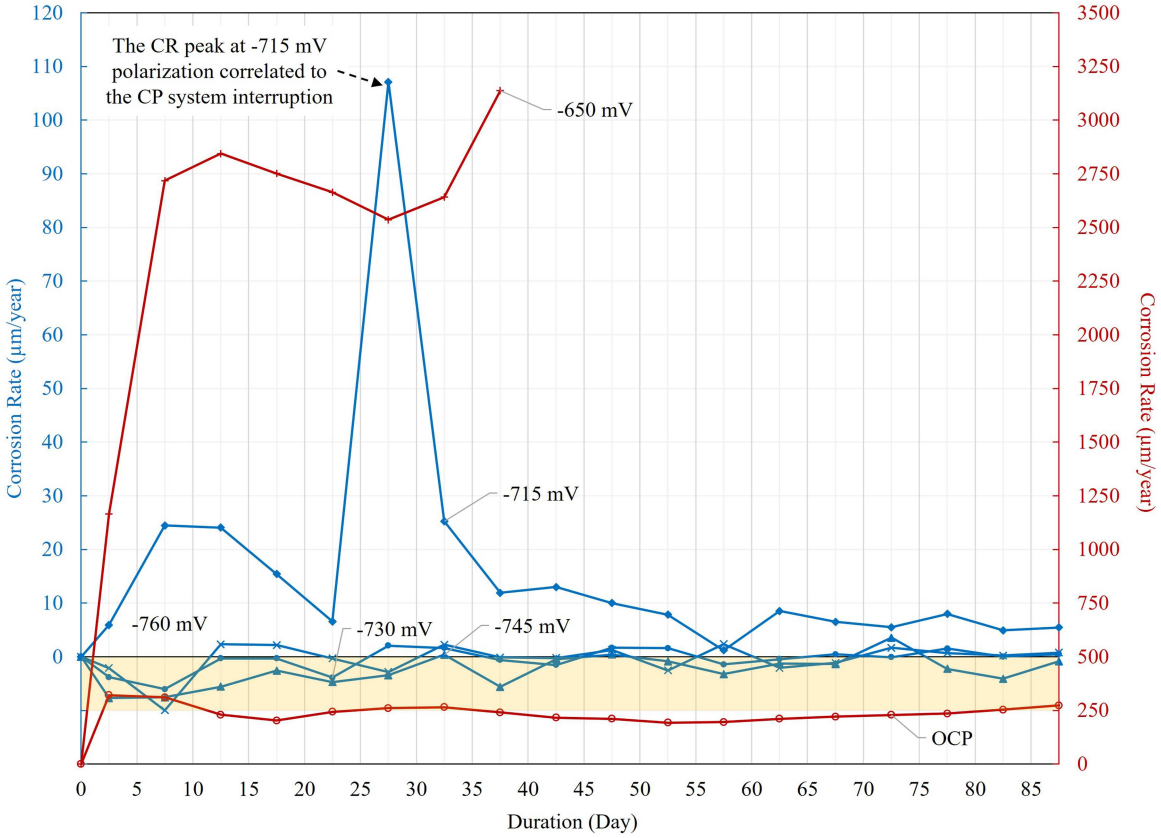

FIGURE 8 | Corrosion rate of ER probes under different polarization conditions throughout the test duration. [Color figure can be viewed at wileyonlinelibrary.com]

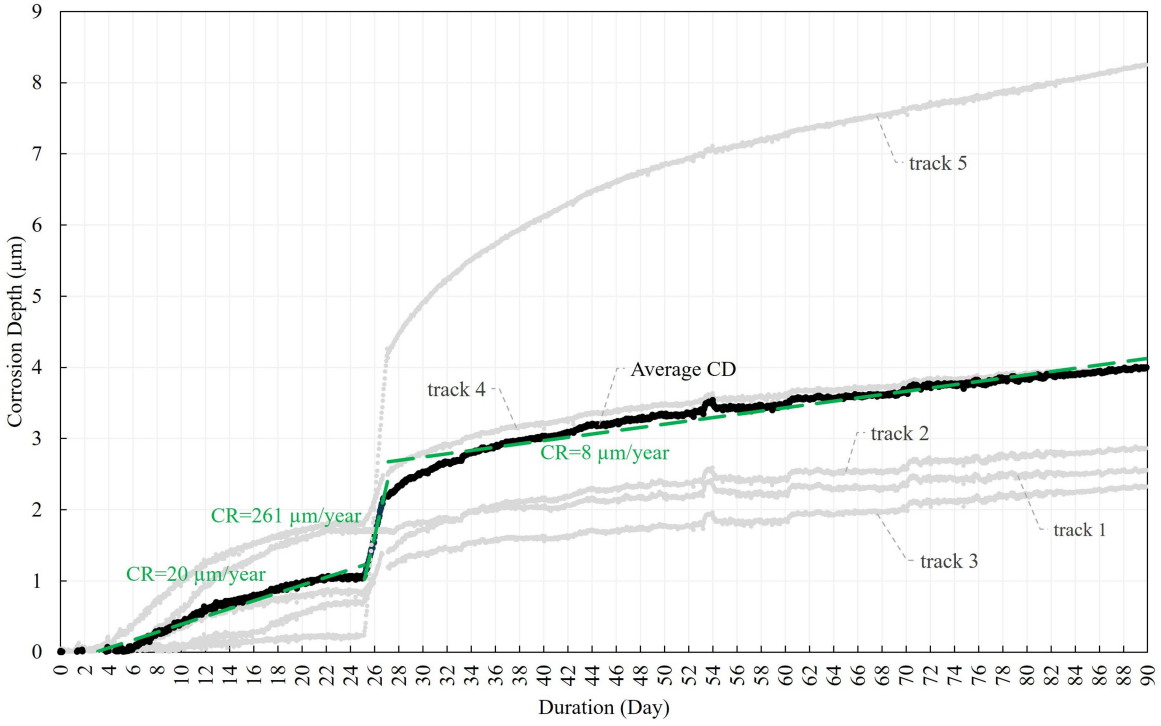

FIGURE 9 | Corrosion depth for the ER probe under −715 mV polarization. [Color figure can be viewed at wileyonlinelibrary.com]

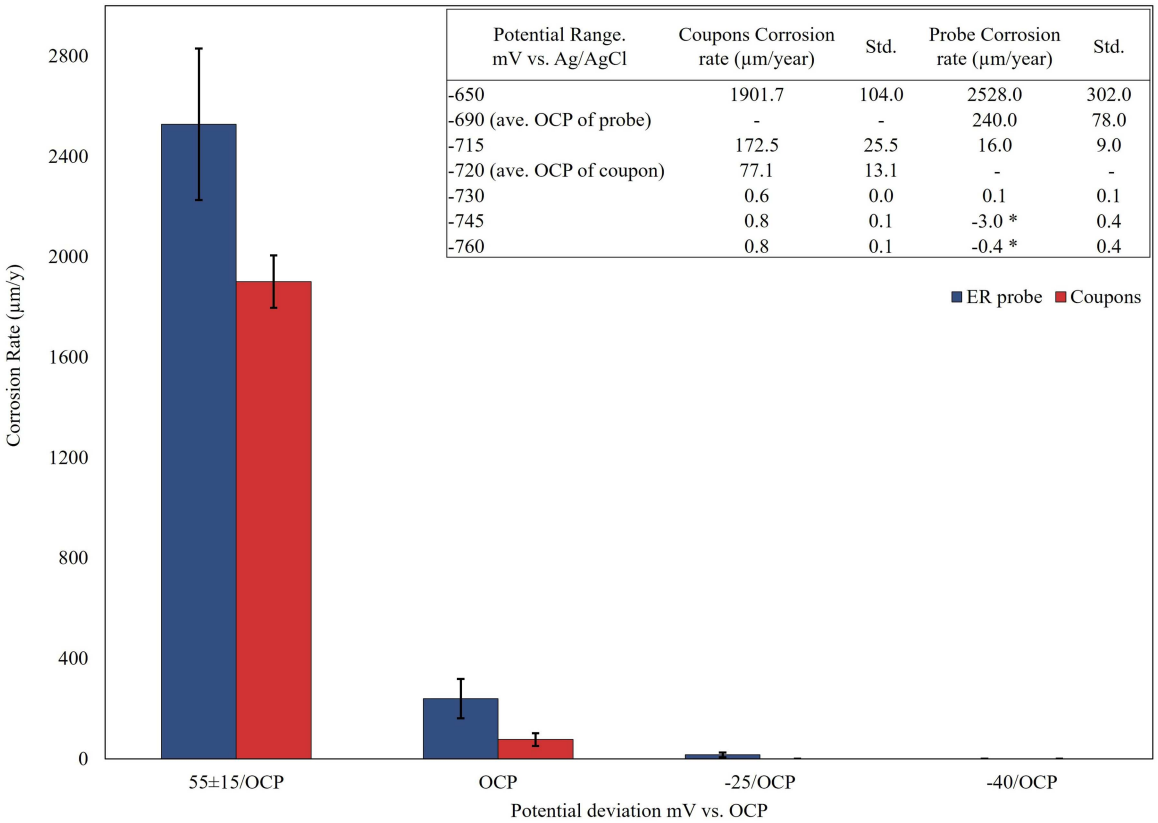

FIGURE 10 | Comparison between the corrosion rates measured by the ER probe with those obtained from wight loss of coupons. *Beyond the setup accuracy. [Color figure can be viewed at wileyonlinelibrary.com]

233 days; and corrosion rates for the other potential levels were determined over 90 days. The standard deviations reported in the table corresponds to five individual coupons for the weight-loss measurements, and to the five tracks of the ER probe for the probe measurements.

Due to the difference in OCP values between the coupon and the ER probe, as confirmed by both the long-term immersion OCP monitoring and the potentiodynamic polarization results (Figure 11a,b), the corrosion rates were compared at equivalent potential deviations relative to the respective OCP of each specimen. This approach ensures a consistent electrochemical basis for performance comparison. The observed divergence in OCP is primarily attributed to differences in geometry and exposed surface area.

In addition, the enclosed table in Figure 10 shows that a slightly negative corrosion rate was obtained by the ER probe at −745 and −760 mV versus Ag/AgCl. Given the 90-day interval used to calculate corrosion rates, the measurement accuracy of the ER probe is approximately 0.3 μm/year; therefore, as noted in Figure 8, values within this accuracy range may appear as small negative rates. Furthermore, the corrosion rates determined from coupon weight loss at −730 mV, −745 mV, and −760 mV versus Ag/AgCl are all below 1 μm/year. Considering the coupon measurement accuracy of 0.2 μm/year for mass losses below 1 mg, these results corroborate the near-zero corrosion rates indicated by the ER probe.

Overall, the probe's high sensitivity and long service life, together with the close agreement between ER-derived and coupon-based corrosion rates, demonstrate that ER probes are reliable tools for corrosion monitoring, particularly for comparative assessments and for evaluating potential-dependent behavior.

ER probes can be affected by interactions between the corrosion product layer and the probe function [3, 8, 21]. This interaction can occur in two ways: (i) an adherent corrosion product layer may create a conductive path for the electric current in parallel with the probe tracks, and (ii) massive corrosion product accumulation (particularly under anodic polarization (Figure 12a) can create a short circuit between different tracks of the probe.

In the first step, a Raman spectroscopy was implemented to analyze the compounds existing in the corrosion product layers formed at different potentials (Figure 12). As can be seen in Table 2, the corrosion product layers contain a range of compounds from conductive ones FeS, Fe_2S, PbS, Fe_3O_4, or MnO_2 to non-conductive ones α-FeOOH, γ-FeOOH, and $CaCO_3$.

To evaluate the potential influence of corrosion products on ER probe measurements, one sensing track was segmented and exposed to seawater under two different polarization conditions: an anodic potential (−650 mV) and a highly cathodic potential (−1100 mV). After 1 month of immersion, the electrical resistance of the track was recorded. Subsequently, all corrosion products were completely removed from the track through a pickling process (see section 2.1), and then it was re-immersed in the same tank under identical environmental conditions, including temperature. The electric resistance was measured again to assess any changes resulting from the removal of corrosion products. As presented in Table 3, the differences in resistance before and after pickling were negligible (less than 1%) on both potentials. This confirms that the

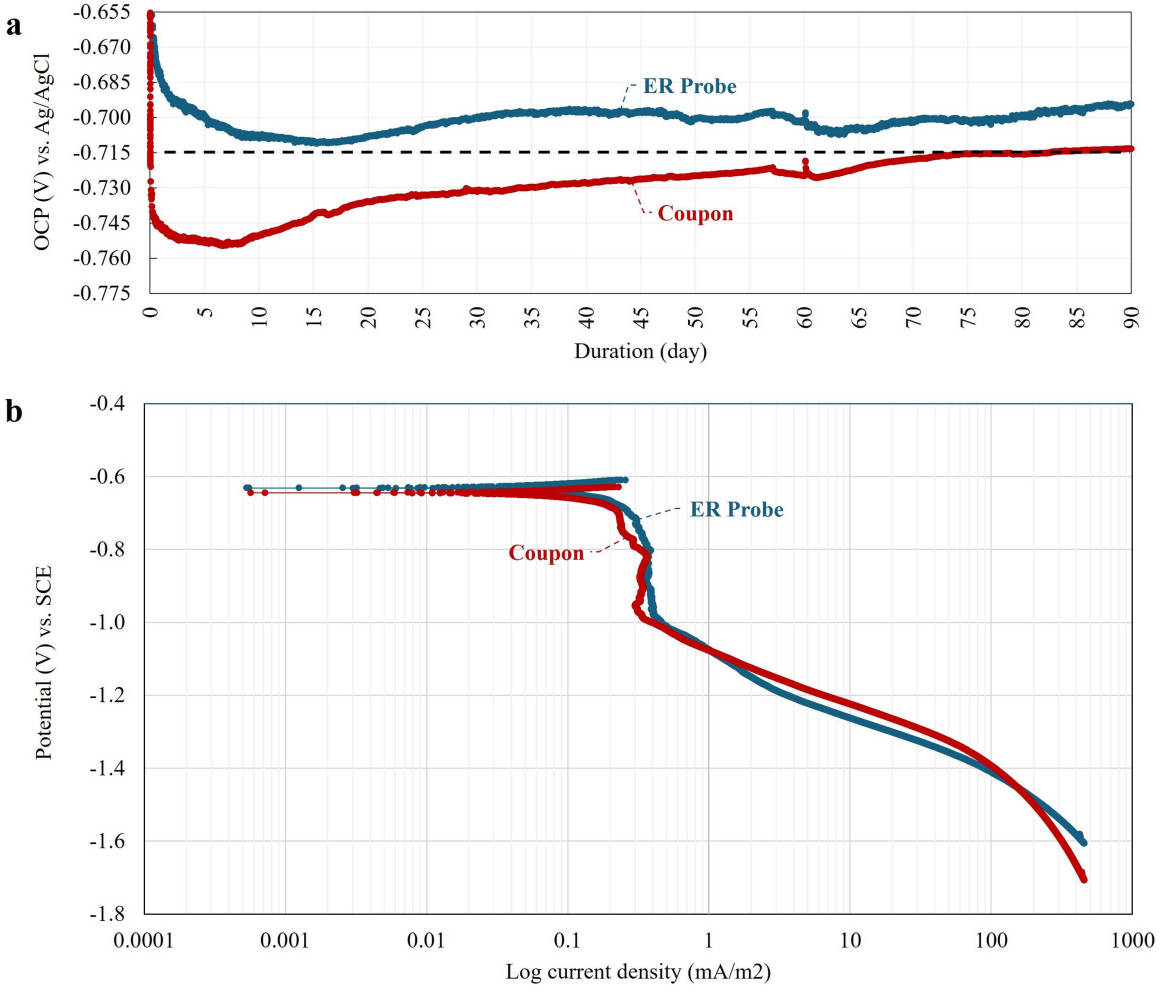

FIGURE 11 | (a) The OCP trend of ER probe and coupons during 90-day immersion, (b) potentiodynamic polarization curves of ER probe and coupon. [Color figure can be viewed at wileyonlinelibrary.com]

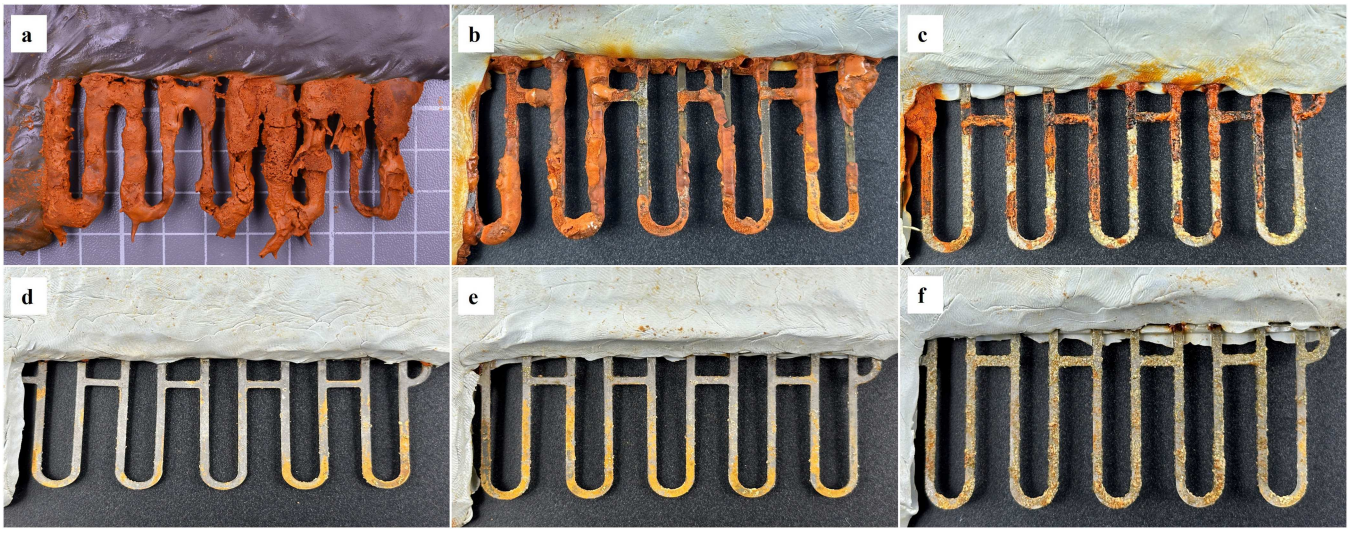

FIGURE 12 | The appearance of the ER probes after 90 days of immersion in natural seawater under different polarization conditions: (a) −650 mV, (b) OCP, (c) −715 mV, (d) −730 mV, (e) −745 mV, (f) −760 mV. [Color figure can be viewed at wileyonlinelibrary.com]

TABLE 2 | Results of Raman spectroscopy on the corrosion products accumulated on the surface of ER probes in different polarization conditions.

Potential	−650 (mV)	OCP	−715 (mV)	−730 (mV)	−745 (mV)	−760 (mV)
Figure no.	12a	12b	12c	12 d	12e	12 f
Corrosion product compounds	• α-FeOOH • γ-FeOOH • FeS • Fe_3O_4	• α-FeOOH • γ-FeOOH • FeS	• α-FeOOH • β-FeOOH • γ-FeOOH • FeS • Fe_3O_4	• α-FeOOH • β-FeOOH • γ-FeOOH • FeS • Amorphous Compound	• α-FeOOH • β-FeOOH • FeS	• FeOOH, nH2O or γ-Fe2O3 or δ-FeOOH • β-FeOOH • FeS • Fe_3O_4 • $CaCO_3$ • Graphite or amorphous carbon • Unidentified organic compound

Note: α-FeOOH: goethite, β-FeOOH: akaganeite, γ-FeOOH: lepidocrocite, FeS: mackinawite, Fe_3O_4: magnetite, $CaCO_3$: calcium carbonate, FeOOH,nH_2O: ferrihydrite, γ-Fe_2O_3: hydrated iron oxide, δ-FeOOH: amorphous iron hydroxide.

TABLE 3 | Measured electrical resistances of one single track with and without the corrosion product layer.

Polarization (mV vs. Ag/AgCl)	Step	Electrical resistance (mΩ)
−650	Initial	6.823
	Before pickling	15.367
	After pickling	15.446
	Difference	0.079
	Discrepancy %	0.5%
	Equivalent corrosion depth (μm)	1.0
−1100	Initial	6.798
	Before pickling	6.811
	After pickling	6.817
	Difference	0.006
	Discrepancy %	0.1%
	Equivalent corrosion depth (μm)	0.3

current track design developed in this study, that is, having a minimum spacing value of 6.18 mm as shown in Figure 3, provides sufficient spacing between tracks, preventing conductive corrosion products from creating a bypass for current flow. Moreover, at −1100 mV versus Ag/AgCl where the massive corrosion product layer does not exist and the tracks bypass is not an issue, the corrosion product removal does not make a considerable change in the registered electrical resistance.

4 | Conclusion

A new ER probe was developed by modifying conventional ER probes design, introducing increased track thickness, multiple sensing tracks, and an adapted corrosion-depth formulation. The corrosion monitoring performance of this novel probe was evaluated under submerged conditions in natural seawater at ambient temperature and benchmarked against those obtained from weight loss measurements of reference coupons. This study demonstrates that the newly developed ER probe provides reliable, real-time corrosion monitoring under submerged natural seawater conditions. The probe successfully captured corrosion-rate variations across a wide potential range, (from −650 to −760 mV vs. Ag/AgCl) simulating galvanic couplings and cathodic protection, and its corrosion-rate trends showed strong agreement with conventional weight-loss measurements. The increased number of tracks improves the measured corrosion rate accuracy and feasibility of non-uniform corrosion detection. The study also shows that the probe's performance remained unaffected by corrosion-product accumulation within the tested spacing design. Overall, our results confirm that this new probe offers a robust, sensitive and reliable tool for quantitative corrosion monitoring and assessment of cathodic-protection performance. The key findings are summarized as follows:

- The probe is able to quantify the impact of an interruption in the cathodic protection system or an under-polarization condition on the corrosion rate.
- A strong correlation was observed between the corrosion rate trends measured by the ER probe and those determined from coupon analysis.
- In this experiment using natural and renewed seawater at lab scale, very low corrosion rate was observed ($< 10\ \mu m/y$) for -760 mV, -745 mV, and -730 mV versus Ag/AgCl potentials which are more electropositive than the protection potential recommended by the ISO 15589-2 standard (-800 mV).
- The accumulation of corrosion products on the probe surface did not measurably interfere with its measurement accuracy.
- Future work should extend its evaluation to other marine exposure zones and compare its capabilities with additional monitoring techniques.

Author Contributions

Mohammad Hassanzadeh: conceptualization, data curation, methodology, formal analysis, investigation, writing – original draft, visualization. **Nicolas Larché:** conceptualization, methodology, writing – review and editing, supervision, resources, validation, project administration, funding acquisition. **Erwan Diler:** conceptualization, methodology, writing – review and editing, resources. **Johan Becker:** conceptualization, methodology, writing – review and editing, resources. **Barbara Rossi:** conceptualization, writing – review and editing, supervision, validation. **Raf Dewil:** conceptualization, writing – review and editing, supervision, funding acquisition, validation.

Acknowledgments

The authors gratefully acknowledge the valuable support provided by the technicians and engineers at French Corrosion Institute. Their assistance with technical guidance and practical expertise was essential for the successful completion of this study. Funded by the European Union (Horizon Europe Marie Skłodowska-Curie Actions Grant Agreement No. 101073471). The views and opinions expressed are, however, those of the authors only and do not necessarily reflect those of the European Union or the European Research Executive Agency. Neither the European Union nor the granting authority can be held responsible for them.

Data Availability Statement

The original contributions presented in the study are included in the article/Supplementary Material; further inquiries can be directed to the corresponding author.

References

1. M. S. B. Reddy, D. Ponnamma, K. K. Sadasivuni, et al., "Sensors in Advancing the Capabilities of Corrosion Detection: A Review," *Sensors and Actuators A: Physical* 332 (2021): 113086, https://doi.org/10.1016/j.sna.2021.113086.

2. K. Popova and T. Prošek, "Corrosion Monitoring in Atmospheric Conditions: A Review," *Metals* 12 (2022): 171, https://doi.org/10.3390/met12020171.

3. X. Sun and L. Yang, Real-time Monitoring of Localized and General Corrosion Rates in Simulated Marine Environments Using Coupled Multielectrode Array Sensors. AMPP, San Diego, 2006, https://doi.org/10.5006/C2006-06284.

4. M. Y. Tan, "A Critical Overview of Monitoring Infrastructural Health Using Corrosion Probes," *Corrosion Engineering Science and Technology* 55 (2020): 103–117, https://doi.org/10.1080/1478422X.2019.1695390.

5. DNV GL, DNV-RP-0416: Corrosion Protection for Wind Turbines, 2016, https://www.dnv.com/energy/standards-guidelines/dnv-rp-0416-corrosion-protection-for-wind-turbines/.

6. A. Groysman, "Corrosion Monitoring," *Corrosion Reviews* 27 (2009): 205–343, https://doi.org/10.1515/CORRREV.2009.27.4-5.205.

7. M. Komary, S. Komarizadehasl, N. Tošić, I. Segura, J. A. Lozano-Galant, and J. Turmo, "Low-Cost Technologies Used in Corrosion Monitoring," *Sensors* 23 (2023): 1309, https://doi.org/10.3390/s23031309.

8. D. H. Xia, C. M. Deng, D. Macdonald, et al., "Electrochemical Measurements Used for Assessment of Corrosion and Protection of Metallic Materials in the Field: A Critical Review," *Journal of Materials Science and Technology* 112 (2022): 151–183, https://doi.org/10.1016/j.jmst.2021.11.004.

9. S. Li, Y. G. Kim, S. Jung, H. S. Song, and S. M. Lee, "Application of Steel Thin Film Electrical Resistance Sensor for In Situ Corrosion Monitoring," *Sensors and Actuators B: Chemical* 120 (2007): 368–377, https://doi.org/10.1016/j.snb.2006.02.029.

10. R. F. Wright, P. Lu, J. Devkota, F. Lu, M. Ziomek-Moroz, and P. R. Ohodnicki, "Corrosion Sensors for Structural Health Monitoring of Oil and Natural Gas Infrastructure: A Review," *Sensors* 19 (2019): 3964, https://doi.org/10.3390/s19183964.

11. C. S. Brossia, K. Chiang, R. A. Cottis, et al., *Techniques for Corrosion Monitoring* (Woodhead Publishing, 2021). 2nd ed., https://doi.org/10.1016/B978-0-08-103003-5.09992-6.

12. K. A. Esaklul and A. L. Ballard, Challenges in the Design of Corrosion and Erosion Monitoring for Deepwater Subsea Equipment – Stretching the Limits of Technology. AMPP, Nashville, 2007, https://doi.org/10.5006/C2007-07338.

13. NACE 3T199: Techniques for Monitoring Corrosion and Related Parameters in Field Applications, 1999, https://content.ampp.org/standards/book/694/Techniques-for-Monitoring-and-Measuring-Corrosion.

14. A. Groysman, "Nondestructive Testing and Corrosion Monitoring." *in: Non-Destructive Evaluation of Corrosion and Corrosion-Assisted Cracking* (Wiley, 2019), https://doi.org/10.1002/9781118987735.ch9.

15. E. Diler, F. Peltier, J. Becker, and D. Thierry, "Real-Time Corrosion Monitoring of Aluminium Alloys Under Chloride-Contaminated Atmospheric Conditions," *Materials and Corrosion* 72 (2021): 1377–1387, https://doi.org/10.1002/maco.202112302.

16. T. Guo, D. Qin, Y. Zou, and Z. Liu, "Research and Development of Corrosion Monitoring Sensor for Bridge Cable Using Electrical Resistance Probes Technique," *Measurement* 237 (2024): 115178, https://doi.org/10.1016/j.measurement.2024.115178.

17. Y. Xu, Y. Huang, X. Wang, and X. Lin, "Experimental Study on Pipeline Internal Corrosion Based on a New Kind of Electrical Resistance Sensor," *Sensors and Actuators B: Chemical* 224 (2016): 37–47, https://doi.org/10.1016/j.snb.2015.10.030.

18. S. Papavinasam, "Monitoring – Internal Corrosion." *Corrosion Control in the Oil and Gas Industry* (Gulf Professional Publishing, 2013), 425–528, https://doi.org/10.1016/B978-0-12-397022-0.00008-X.

19. S. Giriga, U. K. Mudali, V. R. Raju, and B. Raj, "Electrochemical Noise Technique for Corrosion Assessment - A Review," *Corrosion Reviews* 23 (2005): 107–170, https://doi.org/10.1515/CORRREV.2005.23.2-3.107.

20. L. Yang, "Multielectrode systems." *Techniques for Corrosion Monitoring* (Woodhead Publishing, 2021), 173–236, https://doi.org/10.1016/B978-0-08-103003-5.00008-4.

21. V. Vasagar, M. K. Hassan, A. M. Abdullah, et al., "Non-Destructive Techniques for Corrosion Detection: A Review," *Corrosion Engineering, Science and Technology: The International Journal of Corrosion Processes*

and Corrosion Control 59 (2024): 56–85, https://doi.org/10.1177/1478422X241229621.

22. D. Zou, W. Luo, Q. Chen, X. He, and T. Liu, "Corrosion Evolution and Quantitative Corrosion Monitoring of Q355 Steel for Offshore Wind Turbines in Multiple Marine Corrosion Zones," *Ocean Engineering* 311 (2024): 119044, https://doi.org/10.1016/j.oceaneng.2024.119044.

23. M. Dubus, M. Kouril, T.-P. Nguyen, T. Prosek, M. Saheb, and J. Tate, "Monitoring Copper and Silver Corrosion in Different Museum Environments by Electrical Resistance Measurement," *Studies In Conservation* 55 (2010): 121–133, https://doi.org/10.1179/sic.2010.55.2.121.

24. F. Gan, G. Tian, Z. Wan, J. Liao, and W. Li, "Investigation of Pitting Corrosion Monitoring Using Field Signature Method," *Measurement* 82 (2016): 46–54, https://doi.org/10.1016/j.measurement.2015.12.040.

25. X. Sun and L. Yang, Comparison of Oxidation Power Sensor With Coupled Multielectrode Array Sensor for Monitoring General Corrosion. AMPP, Atlanta, 2009, https://doi.org/10.5006/C2009-09443.

26. Y. Kawakam, H. Kanaji, and K. Oku, "Study on Application of Field Signature Method (FSM) to Fatigue Crack Monitoring on Steel Bridges," *Procedia Engineering* 14 (2011): 1059–1064, https://doi.org/10.1016/J.PROENG.2011.07.133.

27. Q. Wang, G. Cong, X. Luo, and P. Xi, "Innovative Magnet-Ultrasonic-Fusion Sensing for Local Corrosion Risk Estimation," *Journal of Loss Prevention in the Process Industries* 98 (2025): 105694, https://doi.org/10.1016/J.JLP.2025.105694.

28. L. Liu, Y. Xu, C. Xu, X. Wang, and Y. Huang, "Detecting and Monitoring Erosion-Corrosion Using Ring Pair Electrical Resistance Sensor in Conjunction With Electrochemical Measurements," *Wear* 428–429 (2019): 328–339, https://doi.org/10.1016/j.wear.2019.03.025.

29. Y. Z. Xu, Y. S. Zhu, L. Liu, L. M. He, X. N. Wang, and Y. Huang, "The Study of the Localized Corrosion Caused by Mineral Deposit Using Novel Designed Multi-Electrode Sensor System," *Materials and Corrosion* 68 (2017): 632–644, https://doi.org/10.1002/maco.201609307.

30. J. Alonso-Valdesueiro, I. Madinabeitia, I. Santos-Pereda, J. B. Jorcin, and E. Acha-Pena, "Highly Sensitive Undersea Corrosion Monitoring System," *IEEE Sensors Journal* 22 (2022): 12278–12287, https://doi.org/10.1109/JSEN.2022.3168364.

31. W. Green, G. Will, J. Katen, and A. Collison, Corrosion Sensors Led In-Service Performance Assessment of Steel Pile Wrapping/Jacketing Systems on Marine Structures in Australia. AMPP, Houston. 2020, https://doi.org/10.5006/C2020-14511.

32. B. Buhr, R. E. Sørensen, A. M. Diederichs, L. P. L. Raun, and Y. Rezania, "Benefits of Corrosion Monitoring for Offshore Wind Structures," *Materials Performance* 62 (2023): 44–48, https://doi.org/10.5006/MP2023_62_11-44.

33. A. J. Olesen, L. R. Hilbert, L. V. Nielsen, and F. Fontenay, Design and Implementation of an Offshore Remote Monitoring System for Corrosion, Coating and Cathodic Protection Performance. AMPP, Denver, 2023, https://doi.org/10.5006/C2023-19265.

34. ISO 15589-1:2015 Standard, Petroleum, Petrochemical and Natural Gas Industries-cathodic Protection of Pipeline Systems, 2015, https://www.iso.org/standard/54503.html.

35. J. Vittonato, N. Larché, E. Diler, and F. Castillon, High Sensitive Sensors for Collection of Cathodic Polarization Data and Determination of Protection Potential Criteria of Buried Structures. AMPP, Nashville.2019, https://doi.org/10.5006/C2019-12896.

36. A. J. Freedman, E. S. Troscinski, and A. Dravnieks, "An Electrical Resistance Method of Corrosion Monitoring In Refinery Equipment," *Corrosion* 14 (1958): 29–32, https://doi.org/10.5006/0010-9312-14.4.29.

37. A. Dravnieks and H. A. Cataldi, "Industrial Applications of a Method For Measuring Small Amounts of Corrosion Without Removal of Corrosion Products," *Corrosion* 10 (1954): 224–230, https://doi.org/10.5006/0010-9312-10.7.224.

38. ASTM G96-90: Standard Guide for Online Monitoring of Corrosion in Plant Equipment (Electrical and Electrochemical Methods), 1990, https://doi.org/10.1520/G0096-90R18.

39. A. Legat, V. Kuhar, M. Leban, and A. Vernekar, Comparison Between Electrochemical Noise and Measurements With Electrical Resistance Probes in Concrete. AMPP, San Diego,2003, https://doi.org/10.5006/C2003-03390.

40. B. Rosborg, A. Kranjc, V. Kuhar, and A. Legat, "Corrosion Rate of Pure Copper in An Oxic Bentonite/Saline Groundwater Environment," *Corrosion Engineering, Science and Technology* 46 (2011): 148–152, https://doi.org/10.1179/1743278210Y.0000000015.

41. T. Prosek, M. Kouril, M. Dubus, et al., "Real-Time Monitoring of Indoor Air Corrosivity in Cultural Heritage Institutions With Metallic Electrical Resistance Sensors," *Studies in Conservation* 58 (2013): 117–128, https://doi.org/10.1179/2047058412Y.0000000080.

42. M. Kouril, T. Prosek, B. Scheffel, and F. Dubois, "High Sensitivity Electrical Resistance Sensors for Indoor Corrosion Monitoring," *Corrosion Engineering Science and Technology* 48 (2013): 282–287, https://doi.org/10.1179/1743278212Y.0000000074.

43. T. Kosec, V. Kuhar, A. Kranjc, V. Malnarič, B. Belingar, and A. Legat, "Development of an Electrical Resistance Sensor From High Strength Steel for Automotive Applications," *Sensors (Switzerland)* 19 (2019): 1956, https://doi.org/10.3390/s19081956.

44. D. Thierry, A. Le Gac, E. Diler, and N. Le Bozec, Recent Advance in Corrosion Monitoring of Atmospheric Corrosion. Proceedings of the Corrosion 2019. AMPP, Nashville. 2019, https://doi.org/10.5006/C2019-12713.

45. E. Diler, F. Lédan, N. LeBozec, and D. Thierry, "Real-Time Monitoring of the Degradation of Metallic and Organic Coatings Using Electrical Resistance Sensors," *Materials and Corrosion* 68 (2017): 1365–1376, https://doi.org/10.1002/maco.201709655.

46. Roxar Retractable ER Probe Data Sheet, RXPS002226, 2018, https://www.emerson.com/en-us/catalog/roxar-retractable-er-probes.

47. F. Martinelli-Orlando and U. Angst, "Monitoring Corrosion Rates With Er-Probes-A Critical Assessment Based on Experiments and Numerical Modelling," *Rights, Corrosion Engineering, Science and Technology* 57 (2022): 254–268, https://doi.org/10.1080/1478422X.2022.2053036.

48. DIN-EN-10130: Cold-Rolled Low Carbon Steel Flat Products for Cold Forming, (1991), https://www.din.de/en/getting-involved/standards-committees/fes/publications/wdc-beuth:din21:91534790.

49. Q.-T. Tran, G. Benoit, O. Le Guennec, and C. Leballeur, Optimization of the Corrosion Protection for Offshore Windfarm Monopile Foundation-Engineering Design Lessons Learnt. AMPP, Nashville. 2019, https://doi.org/10.5006/C2019-13378.

50. M. Marja-aho, P. Rajala, E. Huttunen-Saarivirta, et al., "Copper Corrosion Monitoring by Electrical Resistance Probes in Anoxic Groundwater Environment in the Presence and Absence of Sulfate Reducing Bacteria," *Sensors and Actuators A: Physical.* 274 (2018): 252–261, https://doi.org/10.1016/j.sna.2018.03.018.

51. B. Zajec, M. Bajt Leban, S. Lenart, K. Gavin, and A. Legat, "Electrochemical Impedance and Electrical Resistance Sensors for the Evaluation of Anticorrosive Coating Degradation," *Corrosion Reviews* 35 (2017): 65–74, https://doi.org/10.1515/corrrev-2016-0055.

52. D. Thierry, Final Report of "CORRLOG" Project: Automated Corrosion Sensors as On-line Real Time Process Control Tools, 2008, https://cordis.europa.eu/project/id/18207/reporting/fr.

53. ISO 8407:2021 Corrosion of Metals and Alloys, Removal Of Corrosion Products From Corrosion Test Specimens, 2021, https://www.iso.org/standard/71866.html.

54. ASTM G1: Preparing, Cleaning, and Evaluating Corrosion Test Specimens, 1990, https://doi.org/10.1520/G0001-03R17E01.

55. Service d'Observation en Milieu Littoral (SOMLIT) Webpage, (2024), https://www.somlit.fr/brest/.

56. X. Sun and L. Yang, Real-Time Monitoring of Crevice Corrosion Propagation Rates in Simulated Seawater Using Coupled Multielectrode Array Sensors. Proceedings of the Corrosion. AMPP, San Diego, 2006, https://doi.org/10.5006/C2006-06679.

57. P. Refait, M. Jeannin, R. Sabot, H. Antony, and S. Pineau, "Corrosion and Cathodic Protection of Carbon Steel in the Tidal Zone: Products, Mechanisms and Kinetics," *Corrosion Science* 90 (2015): 375–382, https://doi.org/10.1016/J.CORSCI.2014.10.035.

58. K. Xiao, Z. Li, J. Song, et al., "Effect of Concentrations of Fe2+ and Fe3+ on the Corrosion Behavior of Carbon Steel in Cl− and SO42− Aqueous Environments," *Metals and Materials International* 27 (2021): 2623–2633, https://doi.org/10.1007/s12540-019-00590-y.

59. M. Kouril, T. Prosek, B. Scheffel, and Y. Degres, "Corrosion Monitoring in Archives by the Electrical Resistance Technique," *Journal of Cultural Heritage* 15 (2014): 99–103, https://doi.org/10.1016/j.culher.2013.04.002.